PERGAMON

International Journal of Solids and Structures 36 (1999) 4497–4517

INTERNATIONAL JOURNAL OF SOLIDS and STRUCTURES

Characterization of constraint of fully plastic crack-tip fields in non-hardening materials by the three-term solution

X. K. Zhu, Y. J. Chao*

Department of Mechanical Engineering, University of South Carolina, Columbia, SC 29208, U.S.A.

Received 14 January 1998; in revised form 19 June 1998

Abstract

The J-A_2 three-term asymptotic solution for a crack in a power-law hardening material has been successfully used to interpret the constraint effects due to finite specimen geometry and loading configurations. In the current paper, we study the mechanics behavior of the J-A_2 solution for a plane strain mode-I crack in very low hardening materials. The objective is to investigate the validity of the J-A_2 characterization, in an approximate sense, for the fully plastic crack-tip fields in non-hardening materials. In particular, the constraints at the crack tip for several conventional specimen geometries and loading configurations in non-hardening materials are studied under the framework of the J-A_2 description. The results indicate that within the plastic zone ahead of the crack tip the three-term solution can capture the essential features of fully plastic fields in various finite size specimens in non-hardening materials. Consequently A_2 can be effectively used as a constraint parameter in characterizing the crack-tip field in non-hardening materials.

Keywords: Constraint; Crack-tip field; J-A_2 solution; Slip-line field; Non-hardening material

1. Introduction

The effects of constraint on fracture or crack-tip fields have been widely investigated. Most of the work aims principally at the power-law hardening materials. Among the various constraint parameters proposed, the J-A_2 approach offers a promising methodology to extend the current single parameter, J-based, to a constraint-based, two parameter method for characterizing the fracture event. The present authors (Chao and Zhu, 1998) have summarized in detail the available results of crack-tip fields in hardening materials (e.g. the requirements of HRR singularity or J-dominance conditions) and investigated the J-A_2 characterization of crack-tip fields for the extent

* Corresponding author. E-mail: chao@sc.edu

0020-7683/99/$ - see front matter
PII: S0020-7683(98)00203-0

of J-A_2 dominance and size requirements for fracture testing. Under complete yielding, the analyses based on perfectly plastic fields such as slip-line fields could provide meaningful insights and reference values for low hardening structural materials. Moreover, in non-hardening rigid-plastic materials, the slip-line fields for stationary cracks are useful to the interpretation of growing cracks (McClintock et al., 1995). As such, it is essential to investigate fully plastic crack-tip fields including the constraint effects from geometry and loading configurations in non-hardening materials.

Under fully plastic conditions and using slip-line analysis for perfectly plastic materials, McClintock (1971) first showed that the stress and velocity fields around a notch or crack tip depend on the specimen geometry, crack depth and loading configuration. Although the introduction of strain hardening creates a region over which the HRR singularity dominates, the size of this region strongly depends on both geometry and loading configurations as well as crack length. Thus, generally speaking, a unique 'single parameter' controlling the crack-tip fields exists neither in hardening materials nor in perfectly plastic materials. In the limit of a non-strain-hardening material, both Rice and Rosengren (1968) and Hutchinson (1968) show that the HRR stress field approaches the Prandtl slip-line field at the crack tip for full plasticity. It was further verified under small-scale yielding by the finite element numerical solutions of Rice and Tracey (1973) and Tracey (1976) which reveal the essential feature of the Prandtl field. However, as pointed out by McClintock (1971), the Prandtl field exists only in the crack tip of a double edge deeply notched plate in tension. And the slip-line fields in different notched specimens are generally different and depend on the configurations and the notch or crack length (Green and Hundy, 1956; Green, 1956; Ewing and Hill, 1957; Ewing, 1968; McClintock, 1971). Wu et al. (1990) summarized the slip-line field solutions available for several commonly used fracture test specimens including both deep and shallow cracks. They concluded that the fully plastic crack-tip fields are similar to the Prandtl field for specimens with high triaxiality, e.g. double edged deeply cracked tension, deeply cracked bending and compact tension geometries. But the full plastic-crack-tip fields are considerably different from the Prandtl field for specimens with low triaxiality such as central cracked plate in tension.

Using a modified boundary layer formulation, Du and Hancock (1991) examined numerically the effects of T-stress on the small-scale yielding near-tip field of a crack under plane strain conditions for non-hardening materials. They found that a positive T-stress can cause plasticity to envelop the crack tip and yields the Prandtl field, while a negative T-stress reduces the triaxiality of the stress state at the crack tip and develops an incomplete Prandtl field. Under large-scale yielding, Lee and Parks (1993) carried out the fully plastic analyses of single edge cracked specimens subject to different combined tension and bending for a sufficiently deep crack under plane strain conditions. Kim et al. (1995) performed detailed finite element analyses to study the effects of crack depth on crack-tip constraint at full yielding for plane strain single-edge-cracked specimens under pure bending. These results indicate that only for deep cracks (such as $a/W = 0.5$ and 0.7) under pure bending, the values of crack-tip constraint remain 'almost' constant for all range of deformation levels, and the crack-tip fields are very close to that for the Prandtl field.

In the present work, we investigate the behavior of the J-A_2 three-term asymptotic solutions (Yang et al., 1993) near a crack-tip when the hardening exponent n is very large. These J-A_2 solutions are then used, in an approximate sense, to analyze the constraint behavior at a crack tip for different specimen geometry and loading configurations in non-hardening materials. The objective is to study the validity of using the parameter A_2 to quantify the constraint level at a crack tip in non-hardening materials.

2. Fully plastic crack-tip fields in non-hardening materials

Our attention is confined to mode-I crack problems in non-hardening materials under plane strain conditions. In this section, the Prandtl field is summarized first; then the J-A_2 three-term asymptotic solution for hardening material is reviewed; and finally the J-A_2 three-term solution is extended to nearly non-hardening materials. This J-A_2 three-term solution for nearly non-hardening materials is then used to characterize the fully plastic crack tip fields in non-hardening materials presented in Section 3.

2.1. Prandtl field

The Prandtl field (Prandtl, 1920) is based on the assumption that plasticity completely surrounds the crack tip. On this basis the stresses can be solved by use of slip-line field theory starting from the traction-free crack surface region to the symmetric plane of a tensile crack. The entire field is comprised of three plastic sectors over the crack tip in $0^\circ \leqslant \theta \leqslant 180^\circ$, here θ is a polar angle measured from the remaining ligament of the crack. The three sectors are, respectively, a constant stress sector in $0^\circ \leqslant \theta \leqslant 45^\circ$, a central fan sector in $45^\circ \leqslant \theta \leqslant 135^\circ$ and another constant stress sector in $135^\circ \leqslant \theta \leqslant 180^\circ$. The Prandtl stress field can be expressed, in polar coordinates centered at the crack tip, as follows:

Sector I ($0^\circ \leqslant \theta \leqslant 45^\circ$)

$$\begin{aligned}\sigma_{rr} &= k(1+\pi-\cos 2\theta)\\ \sigma_{\theta\theta} &= k(1+\pi+\cos 2\theta)\\ \sigma_{r\theta} &= k\sin 2\theta\end{aligned} \tag{1}$$

Sector II ($45^\circ \leqslant \theta \leqslant 135^\circ$)

$$\begin{aligned}\sigma_{rr} &= \sigma_{\theta\theta} = k(1+3\pi/2-2\theta)\\ \sigma_{r\theta} &= k\end{aligned} \tag{2}$$

Sector III ($135^\circ \leqslant \theta \leqslant 180^\circ$)

$$\begin{aligned}\sigma_{rr} &= k(1+\cos 2\theta)\\ \sigma_{\theta\theta} &= k(1-\cos 2\theta)\\ \sigma_{r\theta} &= k\sin 2\theta\end{aligned} \tag{3}$$

where $k = \sigma_0/\sqrt{3}$ and σ_0 are the yield strengths in shear and in tension, respectively. The angular distributions of these stresses are shown in Fig. 1 and are independent of the radial distance r from the crack tip.

2.2. J-A_2 three-term asymptotic solution

The general elastic–plastic behavior of hardening materials described by the Ramberg-Osgood power-law stress-strain relation can be written as

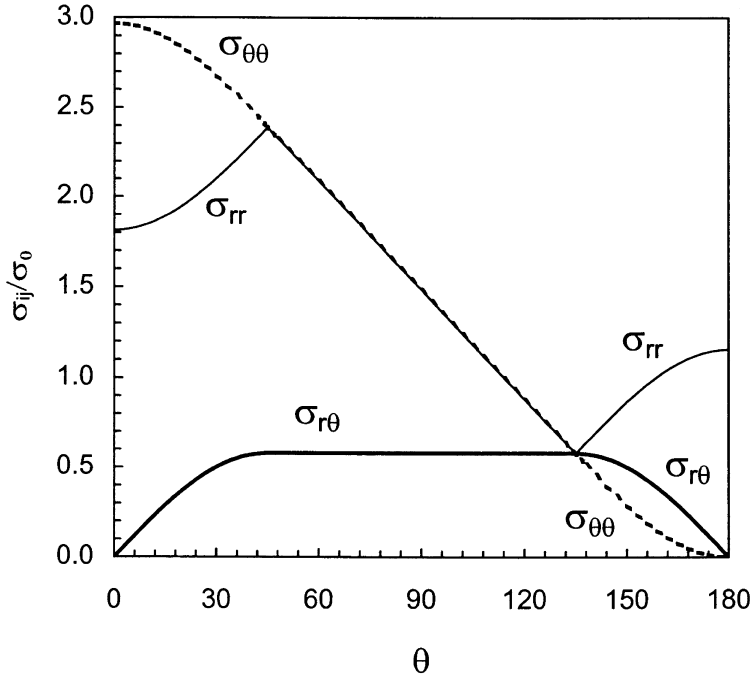

Fig. 1. Stress distributions of Prandtl slip-line field.

$$\frac{\varepsilon}{\varepsilon_0} = \frac{\sigma}{\sigma_0} + \alpha \left(\frac{\sigma}{\sigma_0}\right)^n \tag{4}$$

where ε, σ are the strain and stress in uniaxial tension, σ_0 is a reference stress, $\varepsilon_0 = \sigma_0/E$ is a reference strain with E as Young's modulus, (for actual elastic-plastic solids, σ_0 and ε_0 may be taken to be the yield stress and the yield strain respectively), α is a material constant and n is the strain hardening exponent. From eqn (4) and by use of J_2 deformation plasticity theory, Yang et al. (1993) have developed the following three-term asymptotic crack-tip solutions

$$\frac{\sigma_{ij}}{\sigma_0} = A_1 \left[\left(\frac{r}{L}\right)^{s_1} \tilde{\sigma}_{ij}^{(1)}(\theta, n) + A_2 \left(\frac{r}{L}\right)^{s_2} \tilde{\sigma}_{ij}^{(2)}(\theta, n) + A_2^2 \left(\frac{r}{L}\right)^{s_3} \tilde{\sigma}_{ij}^{(3)}(\theta, n) \right] \tag{5}$$

$$\frac{\varepsilon_{ij}}{\alpha\varepsilon_0} = A_1^n \left[\left(\frac{r}{L}\right)^{ns_1} \tilde{\varepsilon}_{ij}^{(1)}(\theta, n) + A_2 \left(\frac{r}{L}\right)^{(n-1)s_1+s_2} \tilde{\varepsilon}_{ij}^{(2)}(\theta, n) + A_2^2 \left(\frac{r}{L}\right)^{(n-1)s_1+s_3} \tilde{\varepsilon}_{ij}^{*(3)}(\theta, n) \right] \tag{6}$$

where the angular functions $\tilde{\sigma}_{ij}^{(k)}$, $\tilde{\varepsilon}_{ij}^{(k)}$ (in which $\tilde{\varepsilon}_{ij}^{(3)}$ means $\tilde{\varepsilon}_{ij}^{*(3)}$), the stress power exponents s_k ($s_1 < s_2 < s_3$) are only dependent of the hardening exponent n and independent of the other material constants (i.e. α, ε_0, σ_0) and the applied loading. L is a characteristic length parameter which can be chosen as the crack length a, the specimen width W, the thickness B, or unity. The parameters A_1 and s_1 from the HRR fields are given by

$$A_1 = \left(\frac{J}{\alpha\varepsilon_0\sigma_0 I_n L}\right)^{-s_1}, \quad s_1 = -\frac{1}{n+1} \tag{7}$$

and $s_3 = 2s_2 - s_1$ for $n \geqslant 3$. In eqn (7) J is the J-integral (Rice, 1968) and I_n is a dimensionless integration constant. A_2 is an undetermined parameter and may be related to the loading and geometry of specimen. All the non-dimensional functions in eqns (5) and (6) can be found in a report by Chao and Zhang (1997).

From eqns (5) and (6), the three-term expansion of the Mises effective stress $\sigma_e = \sqrt{3s_{ij}s_{ij}/2}$ (where $s_{ij} = \sigma_{ij} - \sigma_{kk}\delta_{ij}/3$) can be expressed by

$$\frac{\sigma_e}{\sigma_0} = A_1\left[\left(\frac{r}{L}\right)^{s_1}\tilde{\sigma}_e^{(1)}(\theta,n) + A_2\left(\frac{r}{L}\right)^{s_2}\tilde{\sigma}_e^{(2)}(\theta,n) + A_2^2\left(\frac{r}{L}\right)^{s_3}\tilde{\sigma}_e^{(3)}(\theta,n)\right] \tag{8}$$

where the angular functions of the effective stress, $\tilde{\sigma}_e^{(k)}(\theta)$, are determined by the angular stress components $\tilde{\sigma}_{ij}^{(k)}(\theta)$ in terms of the following formulae

$$\tilde{\sigma}_e^{(1)}(\theta) = \frac{\sqrt{3}}{2}\sqrt{(\tilde{\sigma}_{11}^{(1)} - \tilde{\sigma}_{22}^{(1)})^2 + 4(\tilde{\sigma}_{12}^{(1)})^2} \tag{9}$$

$$\tilde{\sigma}_e^{(2)}(\theta) = \frac{3}{4\tilde{\sigma}_e^{(1)}}[(\tilde{\sigma}_{11}^{(1)} - \tilde{\sigma}_{22}^{(1)})(\tilde{\sigma}_{11}^{(2)} - \tilde{\sigma}_{22}^{(2)}) + 4\tilde{\sigma}_{12}^{(1)}\tilde{\sigma}_{12}^{(2)}] \tag{10}$$

$$\tilde{\sigma}_e^{(3)}(\theta) = \frac{3}{4\tilde{\sigma}_e^{(1)}}[(\tilde{\sigma}_{11}^{(1)} - \tilde{\sigma}_{22}^{(1)})(\tilde{\sigma}_{11}^{(3)} - \tilde{\sigma}_{22}^{(3)}) + 4\tilde{\sigma}_{12}^{(1)}\tilde{\sigma}_{12}^{(3)}] + \frac{3}{8\tilde{\sigma}_e^{(1)}}[(\tilde{\sigma}_{11}^{(2)} - \tilde{\sigma}_{22}^{(2)})^2 + 4(\tilde{\sigma}_{12}^{(2)})^2] - \frac{1}{2}\frac{(\tilde{\sigma}_e^{(2)})^2}{\tilde{\sigma}_e^{(1)}} \tag{11}$$

When $A_2 = 0$, the three-term asymptotic solutions (5)–(6) reduce to the leading-term HRR singularity solutions. In other words, the first-order field of the three-term asymptotic solutions is the HRR singularity field. Chao et al. (1994) has shown that for moderate to low hardening materials, i.e. $n \geqslant 3$, the above three-term asymptotic solutions (5)–(6) are plastic solutions and can be used to characterize the stress, strain and deformation in the crack tip region which is much larger than the J-dominated region. Furthermore J-A_2 solution is universally valid in both SSY and LSY, low constraint and high constraint crack geometry, and low and high strain hardening materials (Chao and Zhu, 1998).

2.3. The behavior of the three-term asymptotic solution in the limit $n \to \infty$

As pointed out by McClintock (1971), neither the stress nor the strain distributions of the HRR type solutions exist in the limit $n \to \infty$. The reason is that when the hardening exponent n is finite, the governing equations are elliptical; but become hyperbolic for perfect plasticity ($n \to \infty$). For the same reason, both the second and third order angular stress distributions could not exist in the limit $n \to \infty$. Nevertheless, the asymptotic behavior of every term in the three-term solution is meaningful and useful in the study of crack problems in very slow hardening or nearly non-hardening materials.

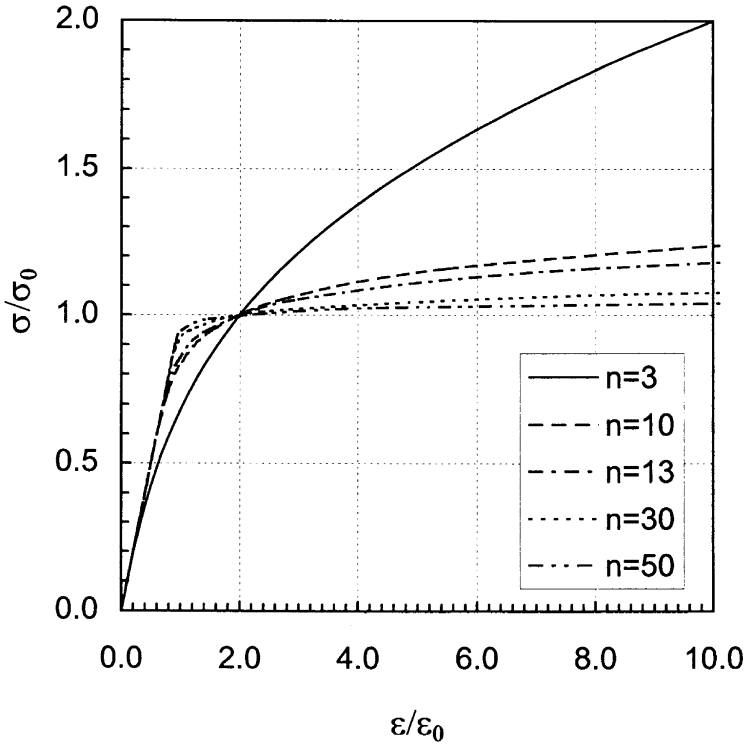

Fig. 2. Ramberg Osgood stress-strain curves in uniaxial tension for hardening exponent $n = 3$, 10, 13, 30 and 50.

From eqn (4) and letting $\alpha = 1$, the stress–strain relation curves with different strain hardening exponent n can be plotted. As shown in Fig. 2, with the increase of the hardening exponent n, the strain-stress curves gradually become flat. We will choose $n = 30$ to approximate the mechanics behavior of perfect plastic material. Note that for $n = 30$ the difference in σ/σ_0 between this material and the perfectly plastic material is only about 7% at $\varepsilon/\varepsilon_0 = 10$. Therefore, it is a reasonable approximation.

For the J-A_2 three-term asymptotic stress field in eqn (5), angular distributions of stress components for each term are illustrated in Figs 3–5 which correspond to $n = 3$, $n = 13$ and $n = 30$, respectively. Except for $n = 3$, stress distributions for each term are nearly similar for $n = 13$ and $n = 30$. Furthermore, the effective stress distributions for each term, i.e. eqns (9)–(11) as shown in Fig. 6 are also similar to each other for $n = 15$, $n = 30$ and $n = 50$. From Fig. 6(a), it is observed that the effective stress for the first term approaches the yield strength with the increase of the hardening exponent n. It is noted that through the comparison of the angular stress variation of the first term in Fig. 4(a) for $n = 13$ and the Prandtl field in Fig. 1, Hutchinson (1968) concluded that the HRR field approaches to the Prandtl field in the limit of a non-strain-hardening material. In fact, further comparing Fig. 5(a) with Fig. 1, one can observe that the angular stress field of the first term in the three-term asymptotic solution, eqn (5), for $n = 30$ is really very close to the Prandtl field. With these comparisons and the fact that the solution for non-hardening material cannot be achieved by letting $n \to \infty$ in the asymptotic solution eqn (5), for strain hardening

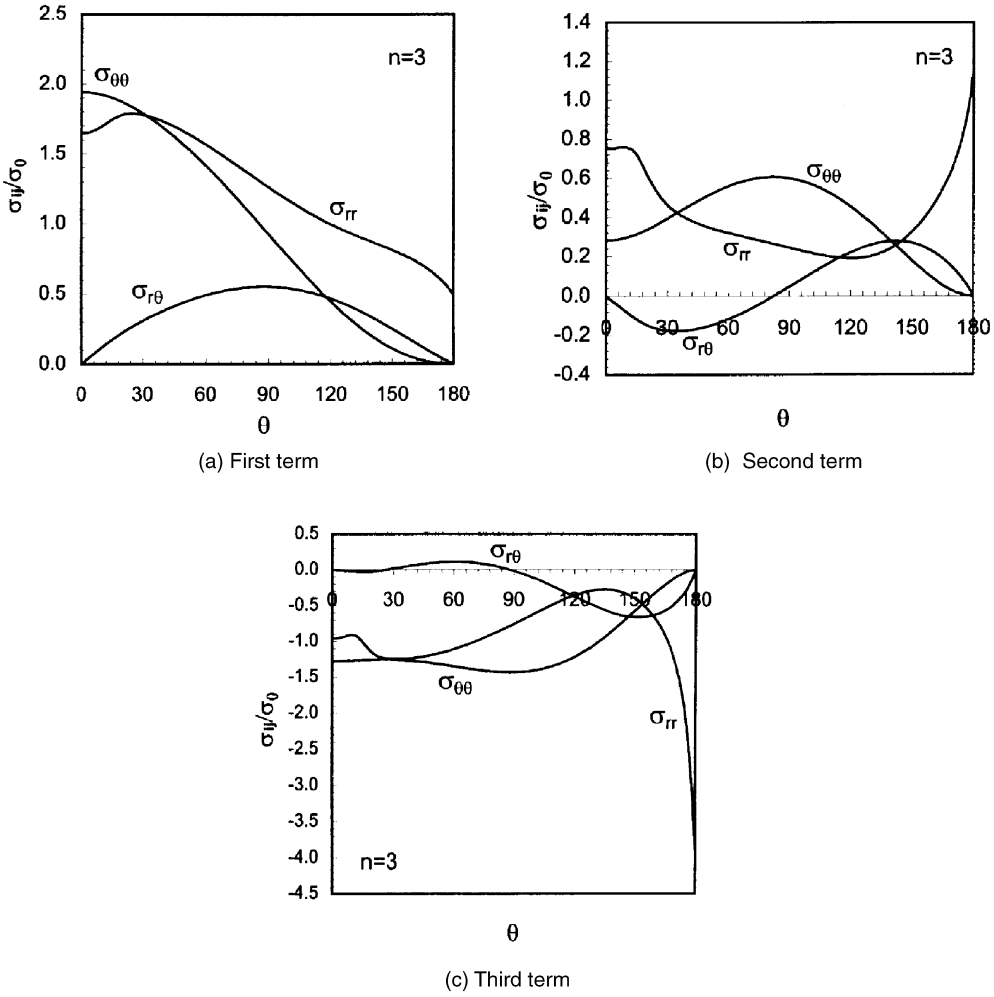

Fig. 3. Angular variations of stress fields in the three-term asymptotic solution with $n = 3$: (a) first order field; (b) second order field; (c) third order field.

materials, we adopt the three-term solution, eqn (5), with $n = 30$ as the approximate solution for non-hardening materials. In addition, as $n \to \infty$ one has $s_1 = s_2 = s_3 = 0$ and $A_1 = 1$ from eqn (7) and Yang et al. (1993). Thus, the stress field in eqn (5) for non-hardening materials can be approximated by

$$\frac{\sigma_{ij}}{\sigma_0} \cong \tilde{\sigma}_{ij}^{(1)}(\theta, n = 30) + A_2\tilde{\sigma}_{ij}^{(2)}(\theta, n = 30) + A_2^2\tilde{\sigma}_{ij}^{(3)}(\theta, n = 30) \tag{12}$$

Furthermore, since our emphasis is placed on the analysis of the constraint effect of non-hardening material we could replace the first term in eqn (12) by the Prandtl solution eqns (1)–(3), to obtain a better approximation to the limiting case $n \to \infty$. Denoting the non-dimensional form of the Prandtl solution by $\tilde{\sigma}_{ij}^{\text{Prandtl}}(\theta) = \sigma_{ij}^{\text{Prandtl}}(\theta)/\sigma_0$, eqn (12) becomes

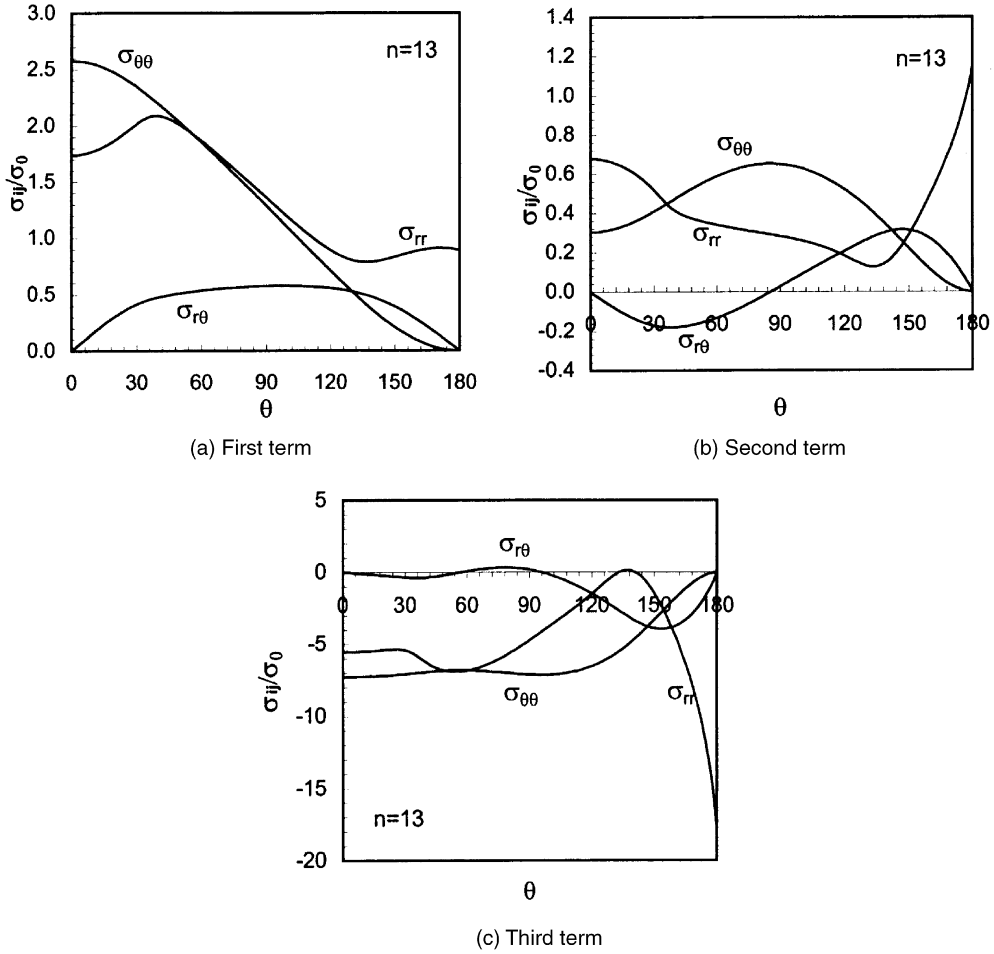

Fig. 4. Angular variations of stress fields in the three-term asymptotic solution with $n = 13$: (a) first order field; (b) second order field; (c) third order field.

$$\frac{\sigma_{ij}}{\sigma_0} \cong \tilde{\sigma}_{ij}^{\text{Prandtl}}(\theta) + A_2\tilde{\sigma}_{ij}^{(2)}(\theta, n = 30) + A_2^2\tilde{\sigma}_{ij}^{(3)}(\theta, n = 30) \tag{13}$$

Equation (13) will be used as an approximate solution for crack-tip fields in the next section to discuss the constraint effect in non-hardening materials. Note that the parameter A_2 in eqn (13) can be determined at a fixed angle, say $\theta = 0^\circ$, by matching one of stress components in eqn (13) with that from a slip-line field or finite element results for a perfectly plastic material. For instance, A_2 can be solved from the following equation

$$\left.\frac{\sigma_{\theta\theta}}{\sigma_0}\right|_{\theta=0} = \tilde{\sigma}_{\theta\theta}^{\text{Prandtl}}(\theta = 0) + A_2\tilde{\sigma}_{\theta\theta}^{(2)}(\theta = 0, n = 30) + A_2^2\tilde{\sigma}_{\theta\theta}^{(3)}(\theta = 0, n = 30) \tag{14}$$

in which $\sigma_{\theta\theta}$ is the crack opening stress ahead of a crack tip in the slip-line field solution or the

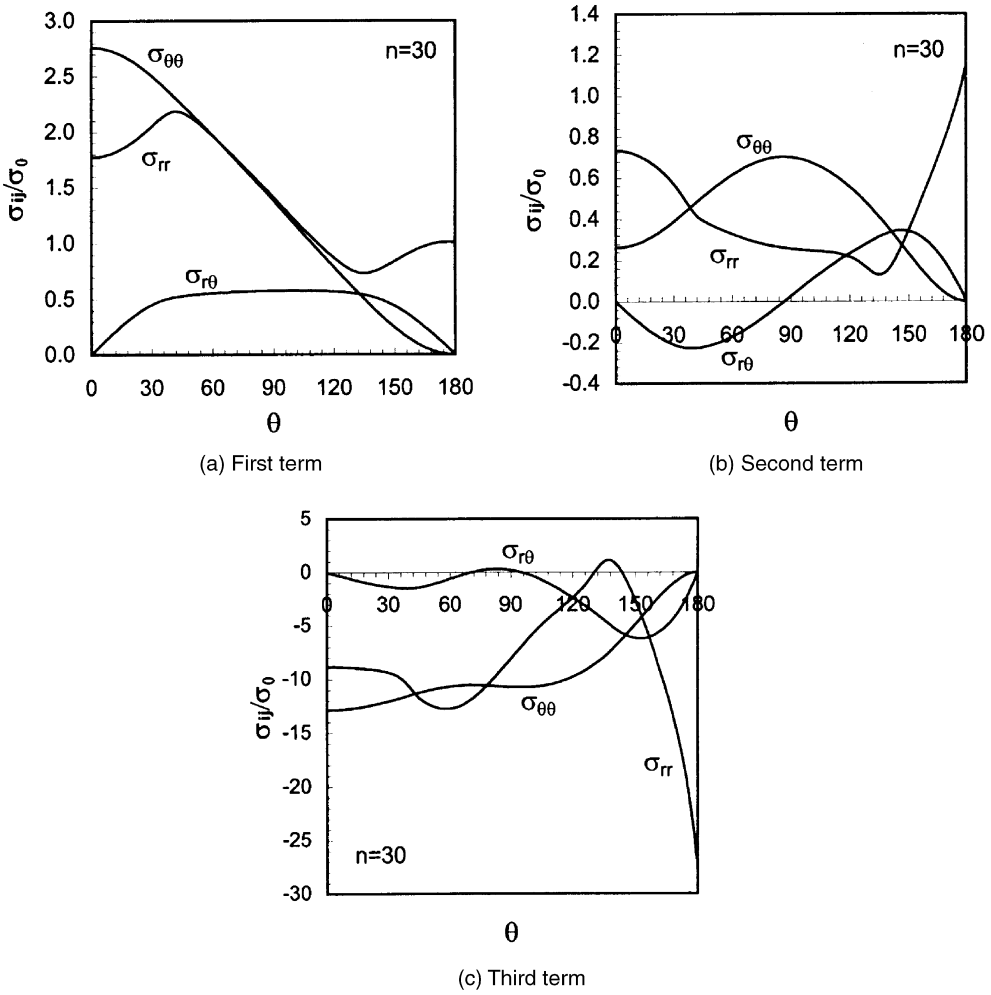

Fig. 5. Angular variations of stress fields in the three-term asymptotic solution with $n = 30$: (a) first order field; (b) second order field; (c) third order field.

finite element numerical solution for a given specimen. Although not reported here, our results from the next section indicate that the approximate results from eqns (12) and (13) are nearly identical.

3. Constraints of crack-tip field characterized by the three-term solution

It should be noted that in eqn (12) or (13) the first term expresses the fully plastic near-tip stress field for a semi-infinite crack in a non-hardening material loaded in Mode I. And the second and the third terms, through the parameter A_2, reflect the influence of finite-sized specimen geometry and loading configuration on the crack-tip fields. Therefore, the parameter A_2 can theoretically

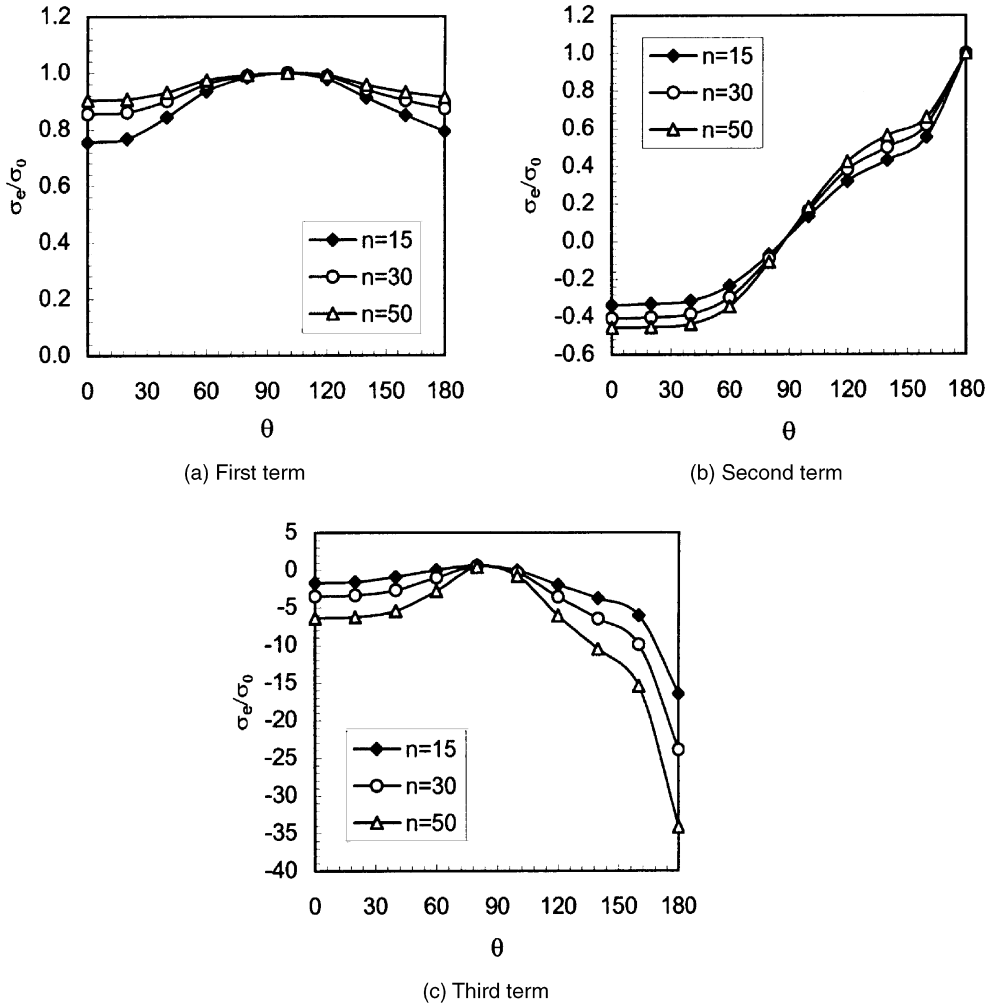

Fig. 6. The angular variations of effective stress σ_e in the three-term asymptotic solution with $n = 15$, 30 and 50: (a) first order field; (b) second order field; (c) third order field.

represent the level of constraint and will be discussed in this section for various finite-sized specimens.

In this section we discuss the constraint effect starting from the small scale yielding case and then to finite-sized specimens. For finite-sized specimens, it is generally acknowledged that a double edge deeply-cracked plate in tension or a single edge deeply-cracked plate under pure bending is the representative for high constraint specimen geometry. And a center-cracked plate under remote tension is the representative for low constraint specimen geometry. The constraints of all other commonly encountered specimen geometries generally fall in between these two extreme cases. As such, our study for finite-sized specimens include a double edge cracked plate in tension, deep and shallow edge cracked plates under pure bending, and center cracked plate under remote tension to

cover a broad range of constraints. Additionally, an edge cracked plate under combined tension and bending is also investigated. Particular emphasis is placed on how well the parameter A_2 can be used to quantify the constraint level over a wide range, say, from pure bending to pure tension.

3.1. Small scale yielding

Under small scale yielding conditions, the plastic zone of the crack tip is very small, but indeed encompasses the entire crack tip in practical structures. In this circumstance, the boundaries of a finite-sized specimen hardly affect the crack-tip fields. For non-hardening materials ($n = \infty$), the finite element results of Shih and German (1981) indicate that as the crack tip is approached the tensile stress ahead of the crack tip in all three specimens (cracked bending bar, single edge cracked panel in tension and center cracked panel in tension) attain the limiting value of 2.97 σ_0 given by the Prandtl field for the case of well-contained plasticity (see Fig. 6 in Shih and German, 1981). For the biaxiality parameter $B = 0$ (or $T = 0$), Betegon and Hancock (1991) and Du and Hancock (1991) presented the crack-tip stress field which is close to the Prandtl field for the non-hardening materials by using a boundary layer approach in their finite element analysis. Consequently, it can be concluded that the crack-tip field in small scale yielding is almost identical to the Prandtl field, or from eqn (13) $A_2 = 0$. In other words, under small scale yielding conditions the crack-tip field is nearly unaffected by the constraints of specimen geometry and loading configuration for non-hardening materials.

3.2. Double edge cracked specimen in tension

A double edge cracked plate specimen loaded by remote tension as sketched in Fig. 7(a) is considered, in which $2W$, $2a$, $2b$ are the width of specimen, the crack length and the ligament length, respectively. When the material is a non-hardening perfectly plastic one, the slip-line field given by Ewing and Hill (1967) shows that for deep cracks or $a/W > 0.884$ the slip-line field is restricted to the remaining ligament and is the well-known Prandtl field; but for $0.770 \leqslant a/W \leqslant 0.884$ the slip-line field is no longer restricted to the ligament and spreads to the free surfaces. For $a/W < 0.770$ there is no strict slip-line field solution. Therefore, for double edge deeply cracked plate in tension with $a/W > 0.884$, the fully plastic crack-tip field is the Prandtl slip-line field in non-hardening material, namely the stresses everywhere in fully yielded ligament are $\sigma_{yy} = (2+\pi)\sigma_0/\sqrt{3}$, $\sigma_{xx} = \pi\sigma_0/\sqrt{3}$, and $\sigma_{xy} = 0$. From eqn (14) we obtain $A_2 = 0$ for this geometry. In addition to $a/W < 0.884$, Ewing and Hill (1967) have also obtained the approximate slip line fields for full range of a/W ratios. Using eqn (13) or (14), A_2 values can be extracted for these cases accordingly.

3.3. Single edge cracked specimen under bending

We consider a single edge cracked plate loaded in pure bending as sketched in Fig. 7(b), in which W, a, b are the width of specimen, the crack length and the ligament length, respectively. For non-hardening materials, Green and Hundy (1956) gave the slip-line solutions for this specimen with deep crack. Green (1956) further pointed out that when the crack length decreases to below a critical length a_c the slip-line field will be no longer restricted to the ligament, but will spread to

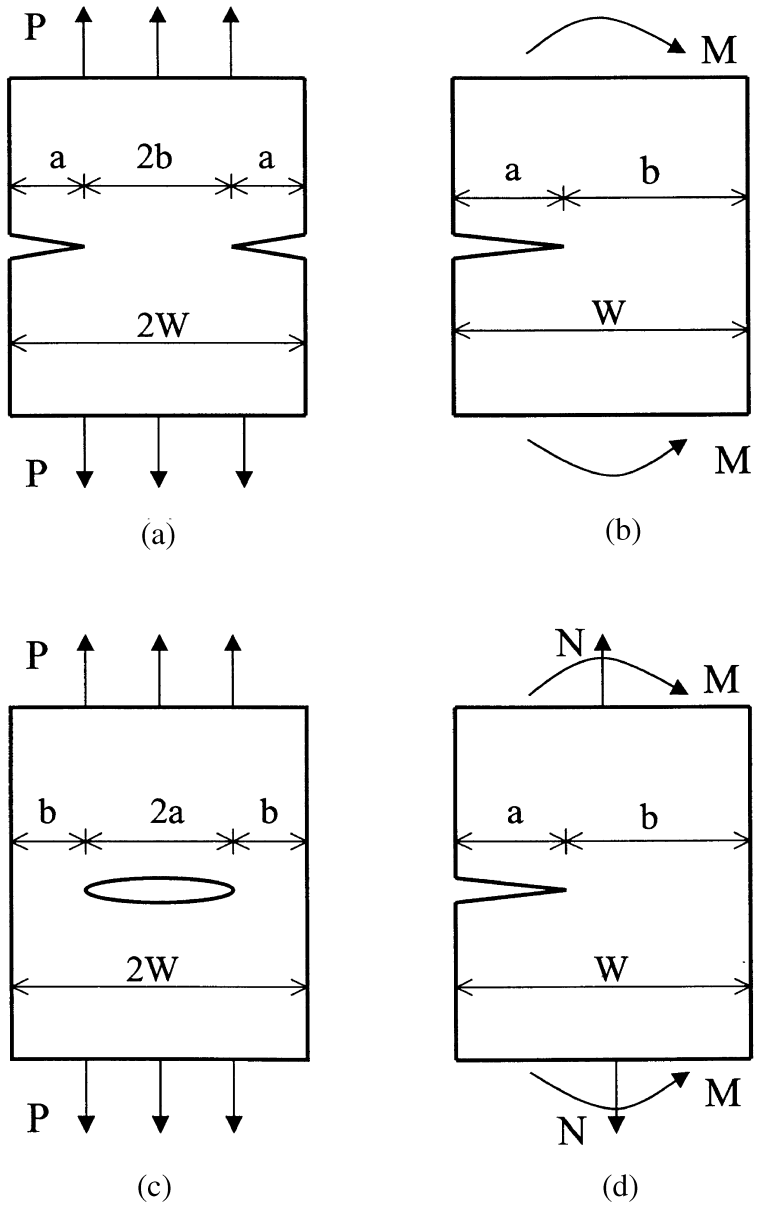

Fig. 7. Cracked specimens considered in the present work.

the specimen free surface on either side of the notches. Ewing (1968) later determined the critical crack length as $a_c/W = 0.297$ and gave the slip-line field solutions for $a/W \leqslant 0.297$ by using a matrix method. Recently, Kim et al. (1996) presented the fully plastic crack-tip fields for these shallow-cracked specimens under pure bending through detailed finite element analyses. Using their numerical results (see Fig. 5 in Kim et al., 1996) and from eqn (14), we can determine the A_2

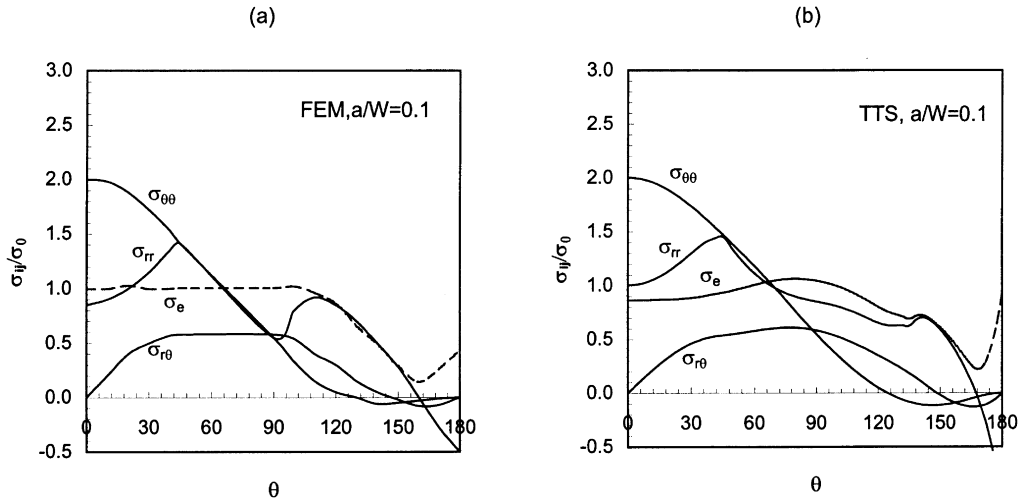

Fig. 8. Stress distributions of single edge cracked specimen in pure bending with $a/W = 0.1$: (a) solution from Finite Element Method (FEM, Kim et al., 1996); (b) Three-Term Solution (TTS, $A_2 = -0.264$).

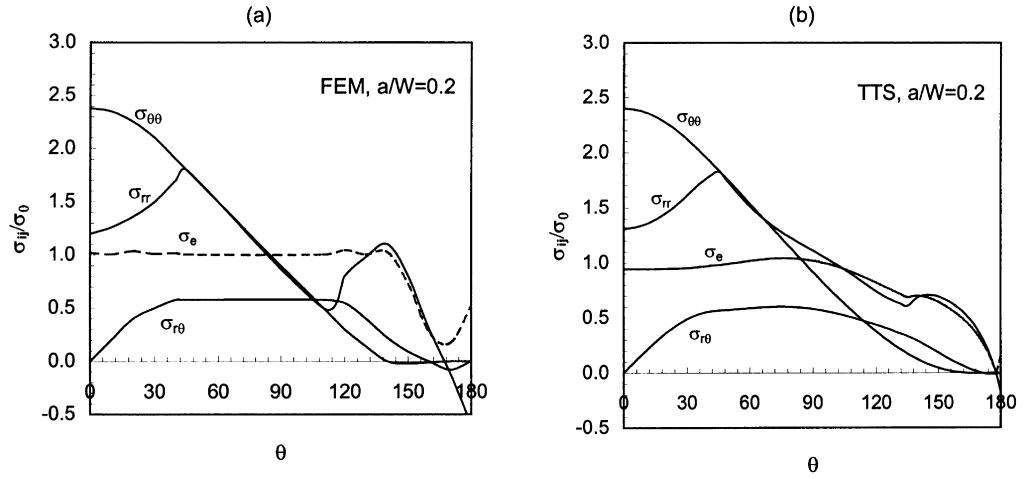

Fig. 9. Stress distributions of single edge cracked specimen in pure bending with $a/W = 0.2$: (a) solution from Finite Element Method (FEM, Kim et al., 1996); (b) Three-Term Solution (TTS, $A_2 = -0.200$).

values for specimens with different a/W ratios. Once the A_2 value is determined, the angular crack-tip stress distributions for a particular specimen can then be obtained from eqn (13).

Figures 8–11 shows the angular distributions of the stress components σ_{rr}, $\sigma_{\theta\theta}$ and $\sigma_{r\theta}$ for this single edge cracked specimen with $a/W = 0.1$, 0.2, 0.3, 0.5 and 0.7 determined from eqn (13) and from Kim et al. (1996) by the finite element method. Figure 12 is the angular variation of the hydrostatic stress or mean stress σ_m for the same specimen. Comparing (a) to (b) in Figs 8–12, it can be concluded that (a) and J-A_2 three-term solution captures the overall trends of the slip-line

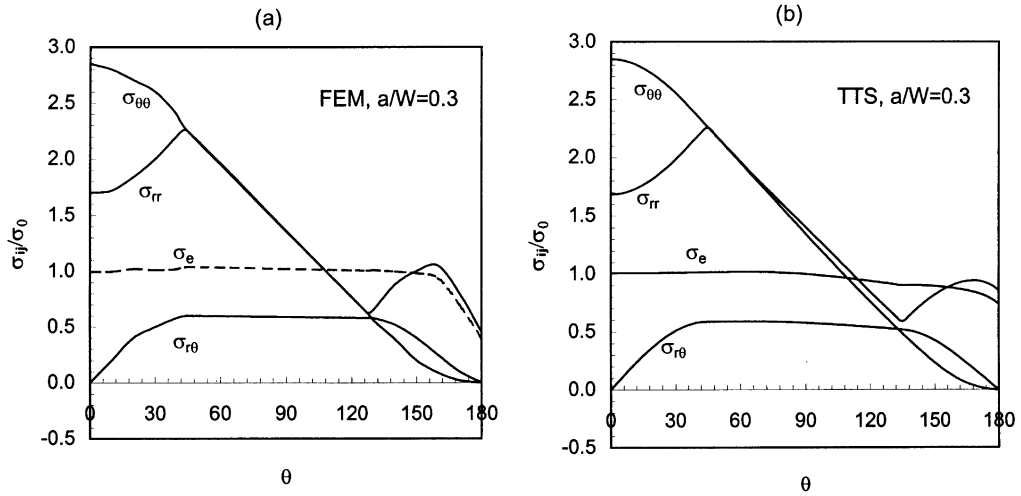

Fig. 10. Stress distributions of single edge cracked specimen in pure bending with $a/W = 0.3$: (a) solution from Finite Element Method (FEM, Kim et al., 1996); (b) Three-Term limit Solution (TTS, $A_2 = -0.086$).

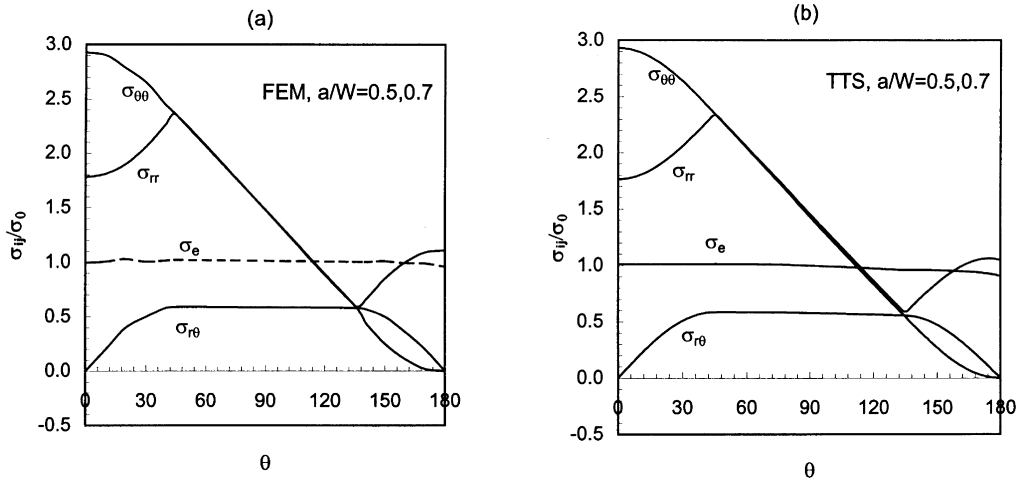

Fig. 11. Stress distributions of single edge cracked specimen in pure bending with $a/W = 0.5$ and 0.7: (a) solution from Finite Element Method (FEM, Kim et al., 1996); (b) Three-Term limit Solution (TTS, $A_2 = -0.045$).

fields for these cases; (b) in the plastic sector, i.e. $\sigma_e/\sigma_0 = 1$, (or at least in the region $0^\circ \leqslant \theta \leqslant 45^\circ$ because in this region the differences of the effective stress σ_e between the three-term solution and the perfectly plastic solution are within 5%) the J-A_2 three-term solutions match quite well with the finite element solutions or the slip-line fields; (c) as the crack becomes 'enough deep', i.e. $a/W \geqslant 0.5$, both the finite element results and the J-A_2 three-term solutions approach the Prandtl fields; (d) the behavior of stress distributions at $a/W = 0.3$ or $A_2 = -0.086$ is indeed the transition between 'deep' and 'shallow' cracks for single edge cracked specimen geometry under bending.

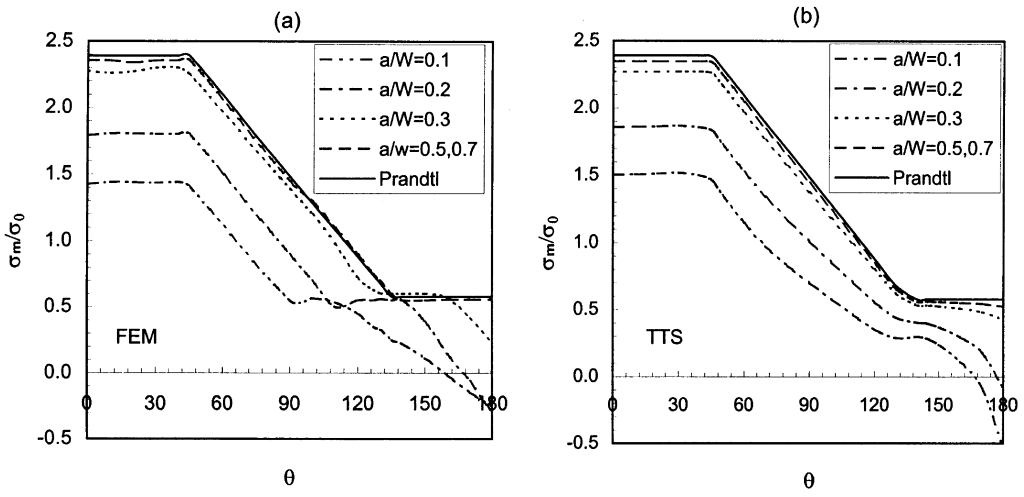

Fig. 12. Hydrostatic stresses of single edge cracked specimen in pure bending for different ratios of a/W: (a) Finite element method solution (FEM, Kim et al., 1996); (b) Three-term solution (TTS, $A_2 = -0.264$, -0.200, -0.086 and -0.045 corresponding to $a/W = 0.1$, 0.2, 0.3, 0.5 and 0.7).

Note that the A_2 value increases with increasing a/W and approaches zero as coming closer to the limiting case, i.e. the Prandtl field. The A_2 values corresponding to $a/W = 0.1$, 0.2, 0.3, 0.5 and 0.7 in Figs 8(b)–11(b) are -0.264, -0.200, -0.086, -0.045 and -0.045, respectively. These values are plotted in Fig. 13 and curve is fitted to yield

$$A_2 = \begin{cases} -1.3295(a/W)^2 + 1.3759(a/W) - 0.3975 & \text{for} \quad a/w < 0.5 \\ -0.045 & \text{for} \quad a/w \geqslant 0.5 \end{cases} \tag{15}$$

Figures 12, 13 and eqn (15) indicate that A_2 value increases with increasing constraint (e.g. large a/W or high stress triaxiality as reflected by the high hydrostatic stress or mean stress σ_m at the crack tip). Therefore, a specimen having low (high) A_2 value implies that it is a low (high) constraint specimen geometry.

3.4. Center cracked specimen under remote tension

In this section we consider a center cracked plate loaded by remote tension as sketched in Fig. 7(c), in which $2W$, $2a$, $2b$ are the width of specimen, the crack length and the ligament length, respectively. For perfectly plastic materials, McClintock (1971) gave the slip-line solution of this specimen as

$$\begin{matrix} \sigma_{yy}(\theta) = 2k \approx 1.1547\sigma_0 \\ \sigma_{xx}(\theta) = 0, \quad \sigma_{xy}(\theta) = 0 \end{matrix}, \quad 0^\circ \leqslant \theta \leqslant 45^\circ \quad \text{and} \quad 0 \leqslant x \leqslant b \tag{16}$$

For a non-hardening material, using the flow theory of plasticity (i.e. taking $\alpha = 1$, $\sigma_0 = 445$ MPa, $\varepsilon_0 = 0.002$ in eqn (4) and $a/W = 0.5$) we performed the finite element calculation for this

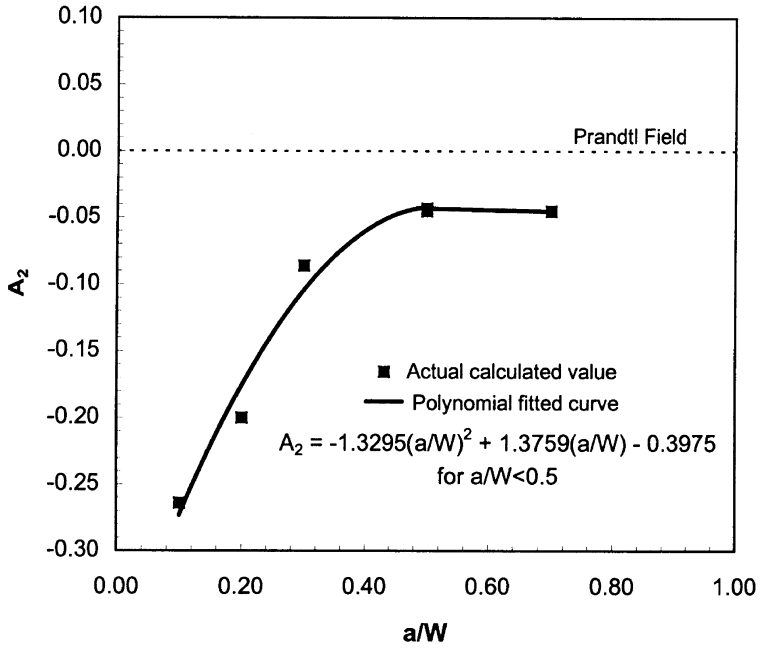

Fig. 13. Variation of A_2 parameter with the crack depth a/W at full plasticity for the single edged cracked specimen under bending.

specimen geometry. Our finite element numerical solutions reveal that the stresses ahead of the crack tip gradually decrease from those in the Prandtl field of eqn (1) toward the slip-line field of eqn (16) with the increasing loading, which is similar to the behavior of a hardening material of $n = 10$ (cf Fig. 8, in O'Dowd and Shih, 1992). At the limit load the stress distributions along the crack ligament are illustrated in Fig. 14. These results are in good agreement with those shown in Fig. 45 of Shih et al. (1979) for the same problem. Comparing Fig. 14 and eqn (16) at $\theta = 0^\circ$, one can see that the stress distributions are close to the slip-line field of eqn (16) only at some distance away from the crack tip. Figure 15(a) illustrates the angular distributions of the stress components around the crack tip at $r \approx 0.05b$ from the finite element analysis. This figure shows that the finite element result (i.e. solid curves) is only close to the slip-line field eqn (16) (i.e. dashed curves) over $0^\circ \leqslant \theta \leqslant 45^\circ$, but not the same.

Using eqn (13) to demonstrate the constraint effect, the curves in Fig. 15(b) are the three-term solutions from eqn (13) determined by matching the $\sigma_{\theta\theta}$ in the finite element analysis at $\theta = 0^\circ$ which yields $A_2 = -0.3477$. Comparing Fig. 15(a) with Fig. 15(b), one finds that the trend of the three-term solutions is similar to the numerical result and the slip-line field in the plastic region $0^\circ \leqslant \theta \leqslant 45^\circ$. Note that in the rigid-plastic analysis for the slip-line field the solution in the plastic region could be unique while the stress distribution in the 'rigid' region may not be unique. Therefore, the comparison in Fig. 15(a) and (b) is only meaningful in the region of $0^\circ \leqslant \theta \leqslant 45^\circ$. However, even in the region $0^\circ \leqslant \theta \leqslant 45^\circ$, the finite element results and the three-term solutions shown in Figs 14 and 15 are not quite the same as the slip-line fields of eqn (16). Further studies can be found in Zhu and Chao (1999) for this particular specimen geometry.

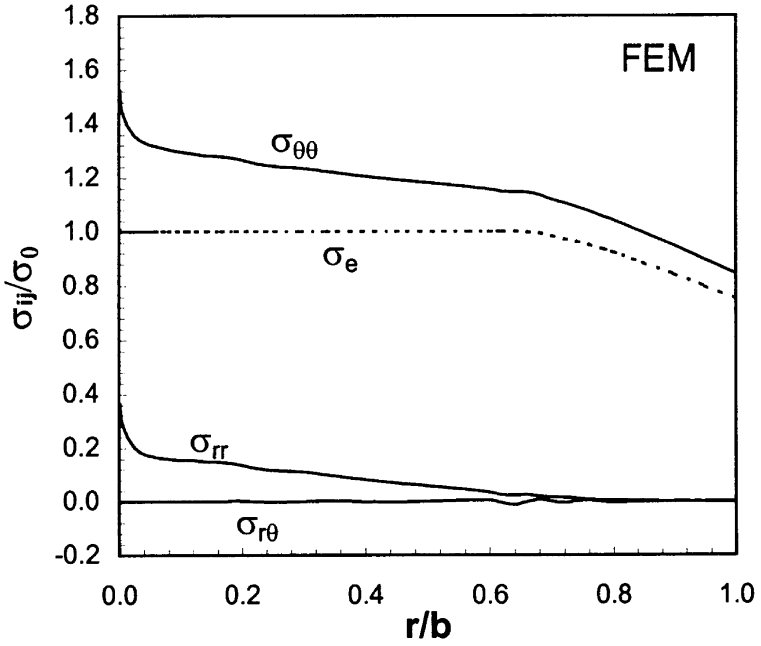

Fig. 14. FEM stress distributions along the crack ligament of center cracked panel in tension with $a/W = 0.5$.

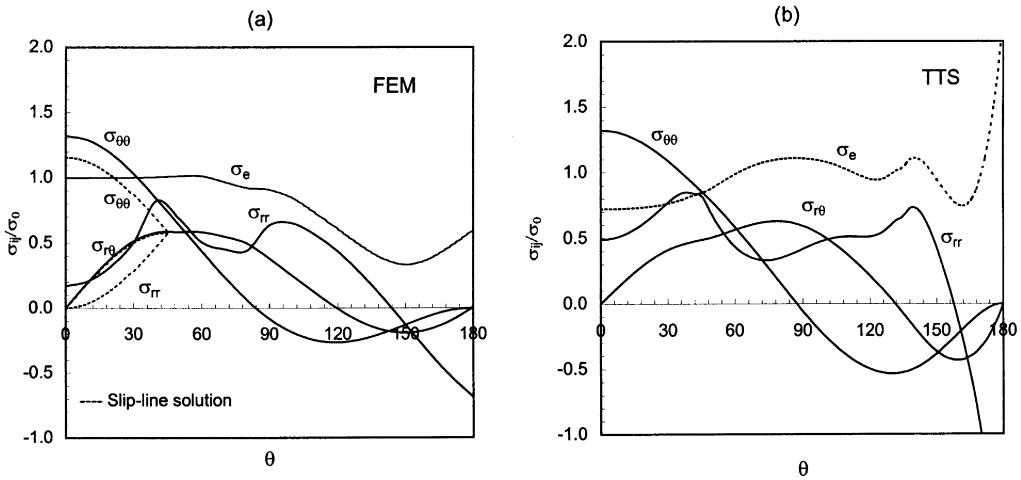

Fig. 15. Angular stress distributions of center cracked panel in tension with $a/W = 0.5$: (a) FEM stresses at $r = 0.05b$ (dash curves represent the slip-line solution); (b) TTS stresses with $A_2 = -0.3477$.

3.5. Single edge cracked panel under combined tension and bending

A single edge cracked plate loaded with combined tension (N) and bending (M) as sketched in Fig. 7(d) is considered in this section, in which W, a, b are the width of specimen, the crack length

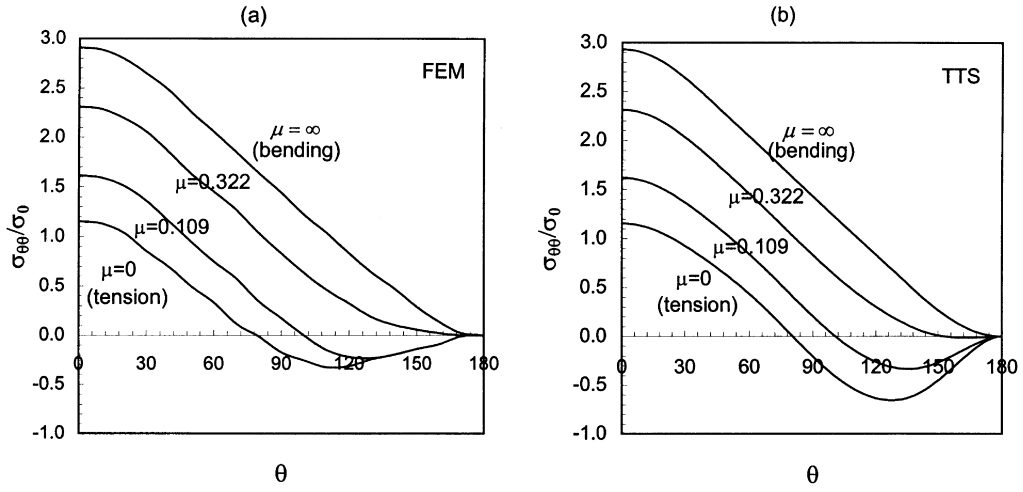

Fig. 16. Angular stress variations of single edge cracked panel with $\mu = 0$, 0.109, 0.332, ∞: (a) solution from Finite Element Method (FEM, Lee and Parks, 1993); (b) Three-Term Solution (TTS, $A_2 = -0.366$, -0.314, -0.216 and -0.045 for the specified μ values).

and the ligament length, respectively. For this specimen Lee and Parks (1993) introduced a parameter

$$\mu = \frac{M + Na/2}{NW}$$

to measure the remotely applied tension-to-bending ratio. Therefore, the value of μ lies between 0 and ∞ with $\mu = 0$ being pure tension and $\mu = \infty$ pure bending. The angular distributions of the circumferential stress at the crack tip from Lee and Parks (1993) for $a/W = 0.5$, and $\mu = 0$, 0.109, 0.332, ∞ are shown in Fig. 16(a). Figure 16(b) shows the corresponding angular stress variations of the three-term solution of eqn (13) where $A_2 = -0.366$, -0.314, -0.216 and -0.045, respectively, using eqn (14). As shown in Fig. 16(a) and (b), the three-term solutions are very close to the finite element results by Lee and Parks (1993). Moreover, both results show the crack opening stress ahead of the crack tip increases from tension to bending which is similar to the behavior in hardening materials. Figure 17 illustrates the angular variation of the J-A_2 three-term solutions in single edge cracked panel. Figure 17(a) is a bending dominated case, with $\mu = 0.332$ and $A_2 = 0.216$, and Fig. 17(b) is a tension dominated case, with $\mu = 0.109$ and $A_2 = -0.314$. In Fig. 17(a), the stress distributions are somewhat similar to the Prandtl field. In Fig. 17(b), the crack-tip fields deviate considerably from the Prandtl field.

Note that A_2 value increases with increasing μ (or increased bending component) and approaches -0.045 as coming closer to the pure bending case. Using the J-A_2 three-term solution of eqn (13) to match the finite element result, one finds that the A_2 values corresponding to $\mu = 0.0$, 0.109, 0.211, 0.322, 0.412, 0.5 and ∞ in Fig. 11 of Lee and Parks (1993) are -0.366, -0.314, -0.263, -0.216, -0.173, -0.136 and -0.045, respectively. These values are plotted in Fig. 18 and the curve is fitted to yield

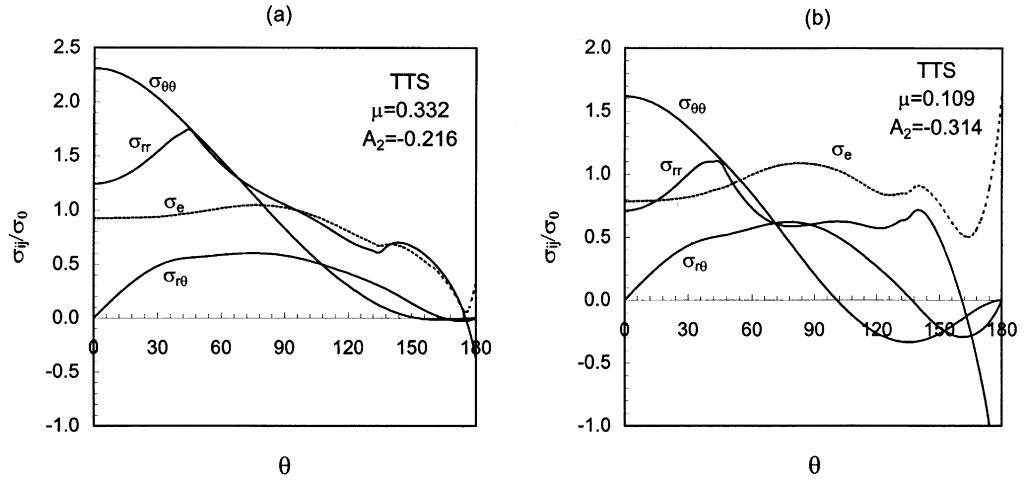

Fig. 17. Angular stress variations of single edge cracked panel using the three-term solutions: (a) the stress with $\mu = 0.332$ and $A_2 = -0.216$; (b) the stress with $\mu = 0.109$ and $A_2 = -0.314$.

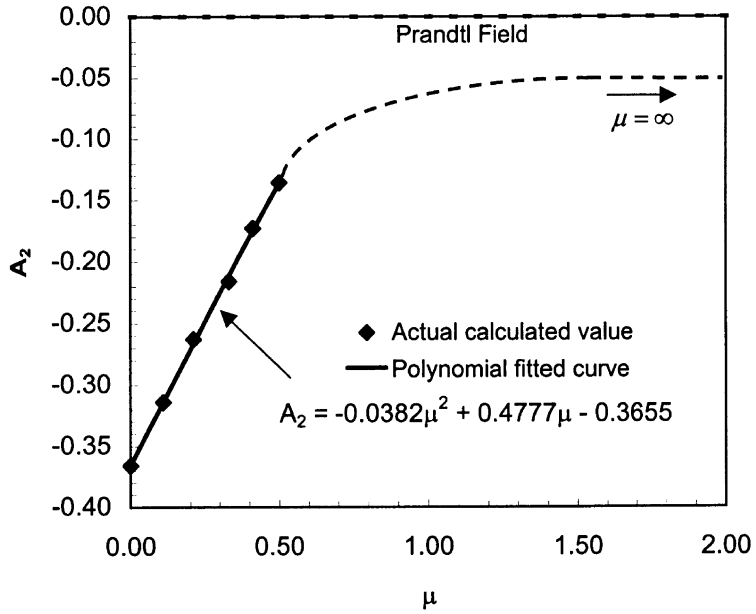

Fig. 18. Variation of A_2 parameter with loading parameter μ from low constraint of tension to high constraint of bending for single edged cracked specimen with $a/W = 0.5$.

$$A_2 = \begin{cases} -0.0382\mu^2 + 0.477\mu - 0.3655 & \text{for} \quad \mu \leqslant 0.5 \\ -0.045 & \text{for} \quad \mu \to \infty \end{cases} \tag{17}$$

Figure 18 shows the variation of A_2 with the constraint for this specimen and loading configuration.

The top dashed line in this figure corresponds to the Prandtl field. Figures 16, 18 and eqn (17) show that for a fixed specimen (i.e. for a fixed a/W) the parameter A_2 or constraint increases as the loading parameter μ increases from zero (pure tension) to infinity (pure bending).

Note that eqn (17) is for $a/W = 0.5$ under various tension to bending ratios. The same procedure can certainly be repeated to generate similar expressions for this type of specimen with other a/W ratios.

4. Conclusions

The mechanics behavior of the J-A_2 three-term solution, originally developed for hardening materials, for a plane strain mode-I crack in very low hardening materials is first studied. An approximate solution for non-hardening materials is developed as an extension of the J-A_2 solution. This J-A_2 solution is then applied to characterizing the constraint behavior of various specimen geometries in non-hardening materials. In particular, the constraints at the crack tip for several conventional specimen geometries and loading configurations in non-hardening materials are studied under the framework of the J-A_2 description. The results indicate that (a) under small scale yielding conditions or in the double edge deeply-cracked specimens under tension, the crack-tip fields are the Prandtl fields corresponding to $A_2 = 0$, and (b) within the plastic zone ahead of the crack tip the J-A_2 three-term solution can capture the essential features of the slip-line fields in various finite-sized specimens in non-hardening materials. Consequently A_2 can be effectively used as a constraint parameter in quantifying the constraint effects for both geometry and loading configuration, and in characterizing the crack-tip field in non-hardening materials, as in the case of hardening materials.

It is interesting to note that mathematically the asymptotic nature of the series solution by Yang, et al. (1993) breaks down in the limit $n \to \infty$ since all terms in the series expansion become equally important, e.g. $s_1 = s_2 = s_3 = \ldots \to 0$. Thus, to effectively reveal the mechanics behavior in the non-hardening case, all terms or many terms from the series expansion must be retained. However, as discovered by Yang, et al. (1993), all the higher order stress terms beyond the second term have similar angular distributions for $n > 3$. As a consequence, the three-term solution, which retains only three terms from the asymptotic series as shown in eqns (5) and (6), is capable of representing more than just three terms and can therefore yield a very good approximation to the full field solution. This argument has been demonstrated for hardening materials by the authors and co-authors in their previous work and is further evidenced by the current paper for non-hardening materials.

Acknowledgements

The authors appreciate the support of this work by NSF through NSF/EPDC$_o$R Cooperative Agreement No. EPS−9630167.

References

Betegon, C., Hancock, J.W., 1991. Two-parameter characterization of elastic-plastic crack-tip fields. Journal of Applied Mechanics 58, 104–110.

Chao, Y.J., Zhang, L., 1997. Tables of plane strain crack tip fields: HRR and higher order terms. ME-Report 97-1, University of South Carolina.

Chao, Y.J, Zhu, X.K., 1998. J-A_2 Characterization of crack-tip fields: extent of J-A_2 dominance and size requirements. International Journal of Fracture (in press).

Chao, Y.J., Yang, S., Sutton, M.A., 1994. On the fracture of solids characterized by one or two parameters: theory and practice. Journal of the Mechanics of Physics and Solids 42, 629–647.

Du, Z.-Z., Hancock, J.W., 1991. The effect of non-singular stresses on crack-tip constraint. Journal of the Mechanics and Physics of Solids 39, 555–567.

Ewing, D.J.F., 1968. Calculations on the bending of rigid/plastic notched bars. Journal of the Mechanics and Physics of Solids 16, 205–213.

Ewing, D.J.F., Hill, R., 1967. The plastic constraint of V-notched bars. Journal of the Mechanics and Physics of Solids 15, 115–121.

Green, A.P., 1956. The plastic yielding of shallow notched bars due to bending. Journal of the Mechanics and Physics of Solids 4, 259–268.

Green, A.P., Hundy, B.B., 1956. Initial plastic yielding in notch bending tests: Journal of the Mechanics and Physics of Solids 4, 128–144.

Hutchinson, J.W., 1968. Plastic stress and strain fields at a crack tip. Journal of the Mechanics and Physics of Solids 16, 337–347.

Kim, Y.-J., Lin, G., Cornec, A., Schwalbe K.-H., 1996. Fully plastic crack-tip fields for plane strain shallow-cracked specimens under pure bending. International Journal of Fracture 78, 21–34.

Lee, H., Parks, D.M., 1993. Fully plastic analyses of plane strain single-edge cracked specimens subject to combined tension and bending. International Journal of Fracture 63, 329–349.

McClintock, F.A., 1971. Plasticity aspects of fracture. In: Leibowitz, H. (Ed.), Fracture: An Advanced Treatise, Vol 3. Academic Press, New York, pp. 47–225.

McClintock, F.A., Kim, Y.-J., Parks, D.M., 1995. A criterion for plane strain, fully plastic, quasi-steady crack growth. International Journal of Fracture 72, 197–221.

O'Dowd, N.P., Shih, C.F., 1992. Family of crack-tip fields characterized by a triaxiality parameter-II. Fracture applications. Journal of the Mechanics and Physics of Solids 40, 939–963.

Prandtl, L., 1920. Ueber die Haerte plastischer Koerper. Goettinger Nachr., math.-phys. Kl. 74–85.

Rice, J.R., 1968. A path independent integral and the approximate analysis of strain concentration by notches and cracks. Journal of Applied Mechanics 35, 379–386.

Rice, J.R., Rosengren, G.F., 1968. Plane strain deformation near a crack tip in a power-law hardening material. Journal of the Mechanics and Physics of Solids 16, 1–12.

Rice, J.R., Tracey, D.M., 1973. Computational fracture mechanics. In: Fenves, S.J. et al. (Eds.), Numerical and Computer Methods in Structural Mechanics. Academic Press, New York, pp. 585–623.

Shih, C.F., German, M.D., 1981. Requirements for a one parameter characterization of crack tip fields by the HRR singularity. International Journal of Fracture 17, 27–43.

Shih, C.F., deLorenzi, H.G., Andrews, W.R., 1979. Studies on crack initiation and stable crack growth. In: Landers, J.D., Begley, J.A., Clarke, G.A. (Eds.), Elastic-Plastic Fracture, ASTM STP 668. American Society for Testing and Materials, pp. 65–120.

Tracey, D.M., 1976. Finite element solutions for crack-tip behavior in small-scale yielding. Journal of Engineering Materials and Technology 146–151.

Wu, S.-X., Mai, Y.-W., Cotterell, B., 1987. Slip-line field solutions of three-point bend specimens with deep notches. International Journal of Mechanical Science 29, 557–564.

Wu, S.-X., Mai, Y.-W., Cotterell, B., 1990. Plastic η-factor (η_p) of fracture specimens with deep and shallow cracks. International Journal of Fracture 45, 1–18.

Yang, S., Chao, Y.J., Sutton, M.A., 1993. Higher order asymptotic crack tip fields in a power-law hardening material. Engineering Fracture Mechanics 45, 1–20.

Zhu, X.K., Chao, Y.J., 1999. Fully plastic crack-tip fields for CCP and DECP specimens under tension in non-hardening materials. International Journal of Solids and Structures (in press).